European Journal of Radiology 157 (2022) 110602

Contents lists available at ScienceDirect

European Journal of Radiology

journal homepage: www.elsevier.com/locate/ejrad

Deep Learning-based calculation of patient size and attenuation surrogates from localizer Image: Toward personalized chest CT protocol optimization

Yazdan Salimi [a], Isaac Shiri [a], Azadeh Akhavanallaf [a], Zahra Mansouri [a], AmirHosein Sanaat [a], Masoumeh Pakbin [b], Mohammadreza Ghasemian [c], Hossein Arabi [a], Habib Zaidi [a,d,e,f,*]

[a] Division of Nuclear Medicine and Molecular Imaging, Geneva University Hospital, CH-1211 Geneva, Switzerland
[b] Imaging Department, Qom University of Medical Sciences, Qum, Iran
[c] Department of Radiology, Shahid Beheshti Hospital, Qom University of Medical Sciences, Qum, Iran
[d] Geneva University Neurocenter, Geneva University, Geneva, Switzerland
[e] Department of Nuclear Medicine and Molecular Imaging, University of Groningen, University Medical Center Groningen, Groningen, Netherlands
[f] Department of Nuclear Medicine, University of Southern Denmark, Odense, Denmark

ARTICLE INFO

Keywords:
X-ray computed tomography
Radiation dose
Deep learning
Phantoms
Body size

ABSTRACT

Purpose: Extracting water equivalent diameter (DW), as a good descriptor of patient size, from the CT localizer before the spiral scan not only minimizes truncation errors due to the limited scan field-of-view but also enables prior size-specific dose estimation as well as scan protocol optimization. This study proposed a unified methodology to measure patient size, shape, and attenuation parameters from a 2D anterior-posterior localizer image using deep learning algorithms without the need for labor-intensive vendor-specific calibration procedures.
Methods: 3D CT chest images and 2D localizers were collected for 4005 patients. A modified U-NET architecture was trained to predict the 3D CT images from their corresponding localizer scans. The algorithm was tested on 648 and 138 external cases with fixed and variable table height positions. To evaluate the performance of the prediction model, structural similarity index measure (SSIM), body area, body contour, Dice index, and water equivalent diameter (DW) were calculated and compared between the predicted 3D CT images and the ground truth (GT) images in a slicewise manner.
Results: The average age of the patients included in this study (1827 male and 1554 female) was 53.8 ± 17.9 (18–120) years. The DW, tube current ,and $CTDI_{vol}$ measured on original axial images in the external 138 cases group were significantly larger than those of the external 648 cases ($P < 0.05$). The SSIM and Dice index calculated between the prediction and GT for body contour were 0.998 ± 0.001 and 0.950 ± 0.016, respectively. The average percentage error in the calculation of DW was 2.7 ± 3.5 %. The error in the DW calculation was more considerable in larger patients (p-value < 0.05).
Conclusions: We developed a model to predict the patient size, shape, and attenuation factors slice-by-slice prior to spiral scanning. The model exhibited remarkable robustness to table height variations. The estimated parameters are helpful for patient dose reduction and protocol optimization.

Abbreviations: CT, Computed tomography; CF, Conversion Factor; AP, Anterior-Posterior; PA, Posterior-Anterior; DW, water equivalent diameter; ED, Effective Dose; TCM, Tube Current Modulation; DL, Deep Learning; $CTDI_{vol}$, Volumetric CT Dose Index; D_{eff}, Effective Diameter; SSDE, Size-Specific Dose Estimate; DLP, Dose Length Product; FOV, Field-of-View; TH, Table Height; GT, Ground truth; RL, Right to Left; CC, Cranio-caudal; SSIM, Structural Similarity Index measure; RAE, Relative Absolute Error; MAE, Mean Absolute Error; BMI, Body Mass Index.

Peer review under responsibility of If file "editor conflict of interest statement" is present in S0, please extract the information and add it as a footnote (star) to the relevant author. The sentence should read (and be amended accordingly): Given his/her role as EditorinChief/Associate Editor/Section Editor <NAME of Editor> had no involvement in the peerreview of this article and has no access to information regarding its peerreview..

* Corresponding author at: Geneva University Hospital, Division of Nuclear Medicine and Molecular Imaging, CH-1211 Geneva, Switzerland.
E-mail address: habib.zaidi@hcuge.ch (H. Zaidi).

https://doi.org/10.1016/j.ejrad.2022.110602
Received 27 April 2022; Received in revised form 2 November 2022; Accepted 6 November 2022
Available online 11 November 2022
0720-048X/© 2022 The Author(s). Published by Elsevier B.V. This is an open access article under the CC BY license (http://creativecommons.org/licenses/by/4.0/).

1. Introduction

X-ray computed tomography (CT) imaging is a powerful tool in the diagnosis and follow-up of various clinical indications in radiology and nuclear medicine departments [1–4]. At the same time, concerns about radiation risks and the hazardous effects of exposure to ionizing radiation are rising[5]. As such, accurate estimation of the radiation dose delivered to patients became an essential component of CT examination procedures toward imaging protocol optimization. In the clinical setting, computed tomography dose index (CTDI) and dose length product (DLP) are the main dose metrics reported on acquisition consoles and patients' radiation dose reports. However, they only describe the CT tube's radiation output regardless of the scanned object [6]. The AAPM report 220 developed the concept of size-specific dose estimate (SSDE) to take into account patient size through considering some conversion factors (CFs) for CTDI to have a more realistic dose estimation in CT [7]. In this regard, the ICRP report 135 [8] confirmed the usefulness of SSDE in the dose optimization process. The CF can be selected based on patient size surrogates, such as effective diameter (D_{eff}) and water equivalent diameter (DW). Using DW has been recommended as the preferred criterion in the definition of CFs, since it takes into account not only patient size but also the tissue composition of the patient's body, especially in body regions with higher tissue inhomogeneities, such as the thorax [9]. The primary barrier on the way of automated implementation of this process is the lack of quantitative CT localizers. The localizer pixel intensities are vendor-specific, and as such, the quantification process requires a stabilized calibration strategy across various vendors.

DW can be calculated using both 3D axial and 2D localizer CT images. 3D CT images provide a more robust and accurate measurement of DW and D_{eff}. However, the input images could be affected by truncation artifacts owing to the limited reconstruction field-of-view (FOV), which is common in thoracic, cardiac, and musculoskeletal CT examinations [10–12]. Besides, it requires more computational and storage resources and is not available before spiral acquisition. Conversely, extracting patient size-related parameters and CFs from the localizer images are not affected by truncation because they are commonly acquired with an extended FOV option and do not need much space and computational burden. In this light, the definition of more accessible and easier metrics for patient attenuation has been suggested by Mihalidis et al. [13]. In addition, patient size and attenuation information extracted from the localizer image can be used to optimize the irradiation parameters according to the desired image quality and radiation dose. Knowledge of the patient's body attenuation or shape characteristics prior to spiral CT scanning is helpful in effectively optimizing spiral CT scanning to achieve automatic tunning of size-adapted exposure parameters, such as automatic tube current modulation (TCM) and automatic kVp selection [14–17]. Ichikawa et al. trained a deep neural network to correlate the scout image and patient's weight with an error close to 3 kg [18]. However, owing to the lack of a standard absolute calibration for the localizer pixel values among different vendors and the limited accuracy, even when using more complex and time-consuming calibration procedures, estimation of DW based on the localizer is not recommended by the AAPM and is not commonly used in a clinical setting. In addition, the magnification/minification of the localizer images caused by altering the table height (TH) is another challenging issue that affects the accuracy and reproducibility of DW measurement [12,19,20].

Zhang et al. [21] calibrated the localizer image according to AAPM report 220 guidelines to obtain accurate localizer pixel values CF to convert the localizer image to DW. Their results showed a 5 % error in phantom measurements. In a follow-up study, they successfully extended the model to different scanners using a single anthropomorphic phantom and five clinical studies [22]. Anam et al. [23] derived a correlation between the water equivalent thickness (T_W) and the AP and lateral localizer image pixel values. They validated their model on body CTDI phantom, an anthropomorphic phantom, and 30 clinical studies, reporting an average error in DW calculation of 5.4 ± 4.2 % compared with axial images serving as ground truth (GT). Burton et al. [24] reported a good agreement between size metrics estimated from two AP and lateral images and the metrics measured from axial CT images on 284 chest CT images with $R^2 = 0.92$. Terashima et al. [20] evaluated the effect of TH on the accuracy of DW estimates from the AP localizer and found a suitable CF based on TH with an error equal to 2.4 % in an anthropomorphic phantom study. Nowik et al. [14] evaluated the radiation dose and functionality of acquiring an ultra-low-dose spiral CT scan before the main spiral CT instead of the 2D localizer within ten patients. They reported accurate size estimation and measurements of DW from the synthetic localizer compared to the routine AP or lateral 2D localizer. The additional radiation dose burden from the additional spiral CT scan was the major drawback of this approach.

Nowadays, machine learning and deep neural networks are being used to solve various problems facing medical imaging, from image denoising, image reconstruction, and segmentation to prognosis and outcome prediction [25–30]. The lack of quantitative CT localizers is the main problem restraining the accuracy and reproducibility, hence preventing the extraction of DW from the localizer image prior to the main scan. The localizer pixel values are vendor-specific, and the quantification process requires a versatile and robust calibration strategy across various vendors. We developed a model to calculate a patient's body shape, size, and attenuation metrics from a single 2D localizer image using deep neural networks to address this limitation.

2. Materials and methods

Extraction of patient size-related parameters prior to CT scanning involved training a deep neural network to predict 3D CT images from the corresponding localizer images. Accordingly, patient-specific body size metrics and attenuation information were extracted from the predicted 3D CT images. These values were then compared to those obtained from standard-dose 3D CT images serving as a standard of reference. The graphical representation of the whole process is illustrated in Fig. 1.

2.1. Study population

This retrospective study included a total of 4005 axial chest CT and localizer images collected from a single center in standard DICOM format. This retrospective study was approved by the ethics committees of the participating center. Written consent was waived with approval. The patients were referred for assessment of various pathologies from 2017 to 2020. All patients were scanned on the Siemens Emotion Duo slice scanner with different tube potentials (kVps) and slice thicknesses. After excluding 624 subjects, 3381 subjects were selected for the final model implementation. The exclusion criteria were arms-down position (96 cases), reconstruction FOV smaller than the patient's body size leading to truncation (459 cases), presence of metallic respiratory aiding equipment in the FOV (12 cases), high-resolution sequential acquisition mode images with table increment more than slice thickness (10 cases), patients scanned in the prone position (38 cases), and patients with low localizer image quality in terms of noise/contrast (9 cases).

2.2. Image Pre-processing

All pre-/post-processing tasks were performed in MatLab 2020b image processing toolbox. According to the location tag in the DICOM header data, the AP localizer images were registered and cropped in craniocaudal (CC) and right to left (RL) directions to the axial image and registered to match 3D axial images. The localizer images were normalized within the range [0–1]. The axial images were resized to 128 (RL) × 64 (CC) pixels.

The axial CT images were registered to the gantry location using the location tag in the DICOM header. Images with a slice thickness of 3 to 8

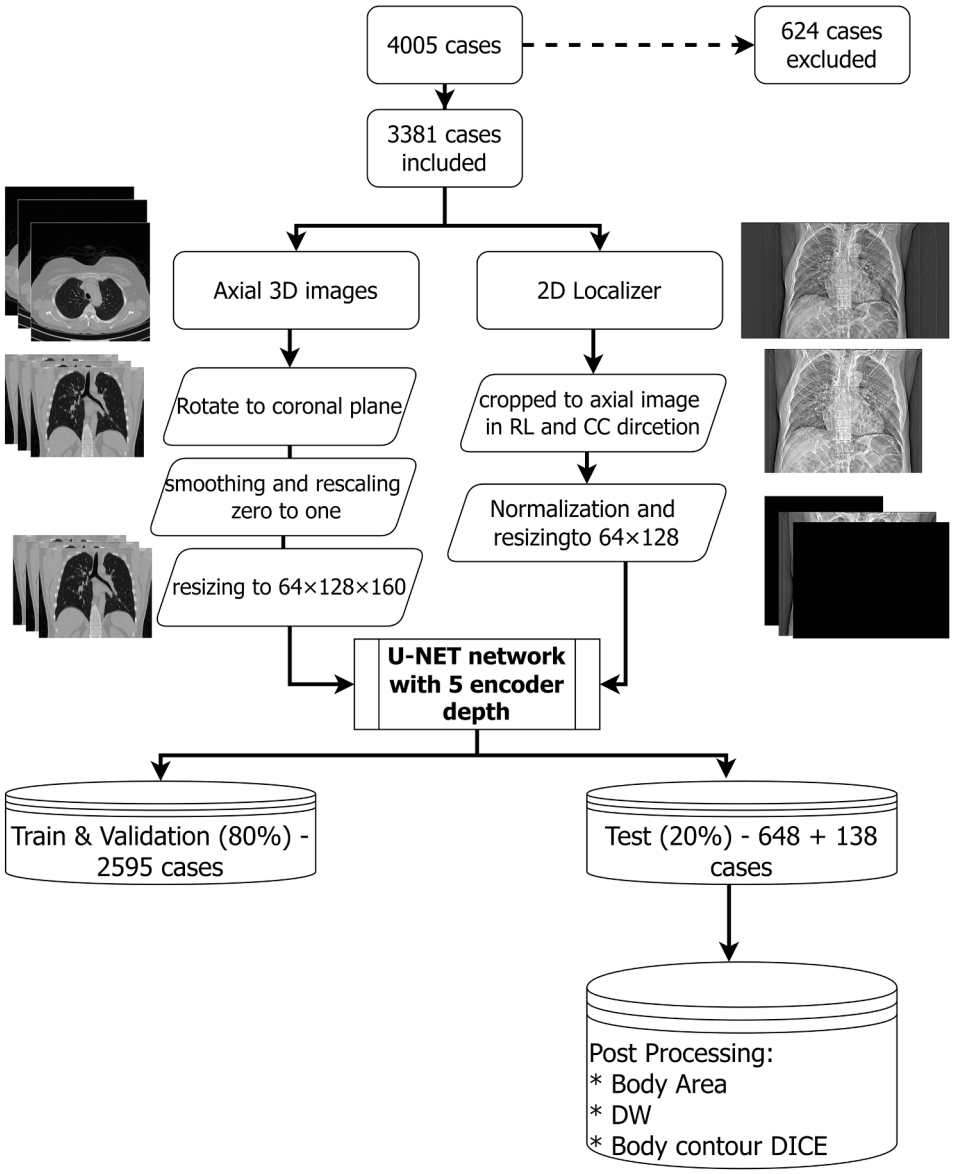

Fig. 1. Flowchart of pre-processing steps and machine learning approach.

mm were cropped in the posterior-anterior (PA) direction by 370 mm coverage in the FOV from a fixed posterior to anterior point of the gantry. After cropping, all images were visually reviewed to verify that a 370 mm PA FOV covers the whole patient's body of all subjects. Then, the axial body contour was extracted, and all voxels outside of the body contour, e.g., the scanner's bed and the blanket in some cases, were replaced by air (-1024 HU). The axial images were smoothed by a 3 mm full-width at half-maximum Gaussian filter in 2D mode. Subsequently, they were rotated to coronal images and resized to 128 (RL) × 168 (PA) × 64 (CC) voxels.

2.3. Network architecture and parameters setting

A modified 3D U-Net-shaped image to image regression network with five encoders and five decoder layers was developed. Each convolutional layer was followed by a max-pooling and a ReLU layer. The training process was performed on Matlab version 2020 (NVIDIA Geforce 2080 Ti GPU with 11 GB of RAM). The localizer images (after pre-processing) were the input, whereas the smoothed coronal images served as the output for the model.

The training of the network was carried out using an L2-norm objective function (OF) along with a regularization L1 term in the following form:

$$OF(regularized) = \frac{1}{2}\sum(\hat{y} - y)^2 + \frac{\lambda}{2}\sum w$$

The following setting was used for the training: optimizer = Adam, learning rate = 0.001, learning rate drop factor = 0.6, learning rate drop period every two epochs, batch size = 2, and decay = 0.00001.

2.4. Implementation details

A total number of 3243 subjects were split into 2270 (70 %) for training, 325 (10 %) for validation, and 648 (20 %) for external tests. From the 3381 cases included in this study, 3243 patients had a fixed table height (TH) equal to 160 mm for both scout scan and 3D axial acquisition, while only 138 cases were scanned using different THs. To evaluate the effect of TH and patient misregistration in the AP direction on the accuracy of our model, we excluded these 138 patients from the training and validation datasets to evaluate the generalizability of our model against this variable through an isolated external validation set. Finally, the model was tested on two separate datasets composed of 648

cases with fixed THs and 138 cases with different THs varying between 80 mm and 230 mm.

2.5. Patient-specific size-related metric calculation

The body contour was delineated by applying intensity thresholding, assessment of shape features within the segmented regions and edge detection, followed by removing the bed and any other object in the field-of-view and hole-filling processing. All body contours were reviewed visually to avoid any potential errors. The DW parameter was calculated based on the protocol reported in the AAPM 220 [7] from axial deep and GT images as the following formula:

$$DW = 2\sqrt{\left[\frac{1}{1000}\overline{CT\ number\ in\ the\ Body\ Contour} + 1\right]\frac{Body\ contour\ Area}{\pi}} \quad (1)$$

where $\overline{CTnumberintheBodyContour}$ is the average of voxel values (HU) in the patient body contour. The evaluation of the model was performed based on two parameters, namely body contour area and DW for the two test groups. The predicted parameters were compared to GT using two strategies. First, total-body patient comparison, wherein the body contour area and DW were averaged on the total number of axial slices. Second, slice-wise comparison, wherein each slice on the predicted image was separately compared with the corresponding slice on the GT image in terms of absolute error. In other words, the evaluation of the model was performed using both patient-wise and slice-wise modes to avoid the averaging effect of negative and positive errors among slices. Besides, the Dice index between the body contour obtained from the model and GT CT images was calculated in a slice-wise mode. In addition, the average HU of the deep learning generated image and the ground truth image within the body contour were compared and the absolute error in HUs (HU_AE) reported.

The average and multiple percentile errors were reported for all parameters. In addition to the R-squared calculated between the DW estimated from the model outcomes and the GT images, other metrics, such as structural similarity index measure (SSIM), mean absolute error (MAE), and relative absolute error (RAE), were calculated in axial mode. Finally, the student's *t*-test was used to compare the statistical significance of the differences between the two groups used as external validation sets (groups with fixed TH (648 cases) and variable TH (138 cases)).

As an estimation of the TCM performance, we calculated DW slice-wise on the 3243 original axial CT images with 512 × 512 pixels size, and the corresponding tube current recorded in each DICOM header was extracted. These values were plotted to find the TCM behavior in clinical conditions.

3. Results

The average age of the patients included in this study (1827 male and 1554 female) was 53.8 ± 17.9 (18–120) years. A tube current of 170.9 ± 38.5 (44–239) mA and kVp of 80 and 110 were used for CT acquisitions with slice thicknesses varying between 2 and 5 mm. Patient demographic and acquisition information was summarized in Table 1. The DW, tube current, and $CTDI_{vol}$ measured on original axial images in the external 138 cases group were significantly larger than those of the external 648 cases ($P < 0.05$). Fig. 2 shows two examples of predicted images versus reference images (axial slices). The visual assessment of automatic analytic body contour definition on axial images confirmed that the process was successful on all included cases.

By comparing the predicted images to the corresponding GT, oriented in the axial view, the average of SSIM, RMSE, RE, ARE, and HU_AE metrics were 0.998 ± 0.001, 0.125 ± 0.027, 0.281 ± 2.626, 7.688 ± 1.955, and 52.1 ± 34.3, respectively. Table 2 summarizes the results of the evaluated metrics in two external validation groups. The average slice-wise Dice index for body contour was 0.948 ± 0.02 (5 percentile = 0.916, 95 percentile = 0.973), reflecting a good slice-wise agreement of body shape prediction. The mean relative errors for DW were 2.9 ± 3.7 % (5 percentile = -3.1, 95 percentile = 9.0 %) and 9.6 ± 5.2 % (5 percentile = 3.5, 95 percentile = 19.5 mm) for total and slice-wise evaluations, respectively.

Fig. 2 shows representative examples of slice-wise DW graphs for four patients with various body habitus. Patients #1 and #2 (upper row) represent two cases with large body sizes (BMI > 30), whereas patients #3 and #4 represent two cases with small body sizes (BMI < 30). The DW scales in the Y direction are not the same for a better illustration of the difference between DL and GT DW. Body habitus can be seen in the lower 3D rendered image. Patients #1 and #4 are female, whereas patients #2 and #3 are male subjects. The excellent agreement between the two methods was observed in the majority of slices.

Fig. 3 shows the histogram distribution of the total errors in DW calculation by the proposed method. The slice-wise relative error for the body area was about 4.0 ± 2.5 % (5 percentile = 1.3, 95 percentile = 8.4 %).

Fig. 4 shows the correlation between DW estimated by the deep learning model and the GT images, wherein R-squared was equal to 0.92, reflecting excellent agreement. A significant correlation between patients' size in terms of DW and the error in the DW estimation was observed, wherein more significant errors were seen for larger patients.

Fig. 5 depicts the tube current vs DW variation in each slice for 112′249 axial slices acquired with 110 kVp, and CareDose TCM turned on. Two linear and exponential curves fitted on the data are shown with R^2 equal to 0.52 and 0.48, respectively.

4. Discussion

This study proposed a new DL-based solution to calculate patient size and attenuation metrics in chest CT scanning from the localizer image. We developed a modified UNET architecture to generate 3D axial images from 2D AP localizers on a large dataset consisting of 3243 chest CT images. We evaluated the trained model on 648 + 138 external validation cases. We assessed the performance of the proposed method in terms of image similarity indices, estimated patient size, shape metrics of body contour, Dice index, and attenuation factors, in addition to the widely accepted metric of water equivalent diameter. In addition to patient-wise analysis (considering the whole patient volume as a single data point), the model's performance was assessed slice by slice to evaluate the feasibility of our proposed method in calibrating a personalized scan parameter modulation. To the best of our knowledge, this is the first AI-based DW size metric estimation from the localizer image performed on a large number of clinical studies.

During the data selection process, we excluded 459 cases (~12 %) from our study because of truncated CT axial images, which reflects the high prevalence of truncation phenomena as reported in previous thoracic CT studies (>80 % of cases) [10]. This fact necessitates finding

Table 1
Demographic data of all 3243 patients included in this study. The DW was measured on original axial images.

Database	Male	Female	Age	Average tube current	$CTDI_{vol}$	DW	kVp
All 4005 cases	1827	1554	53.8 ± 17.9 (18–120)	170.9 ± 38.5 (44.7–239)	4.80 ± 1.15 (1.25–6.89)	30.9 ± 3.65 (17.29 – 42.10)	80 & 110
648 fixed TH Cases	396	252	49.5 ± 14.3 (21 – 87)	165.3 ± 53.3 (54 – 210)	4.62 ± 1.23 (1.34 – 6.70)	30.12 ± 4.31 (17.84 – 39.50)	80 & 110
138 varied TH cases	65	73	55.3 ± 16.5 (27 – 103)	178 ± 42.2 (68–239)	5.15 ± 1.31 (1.51 – 7.02)	32.10 ± 3.84 (19.25 – 42.10)	80 & 110

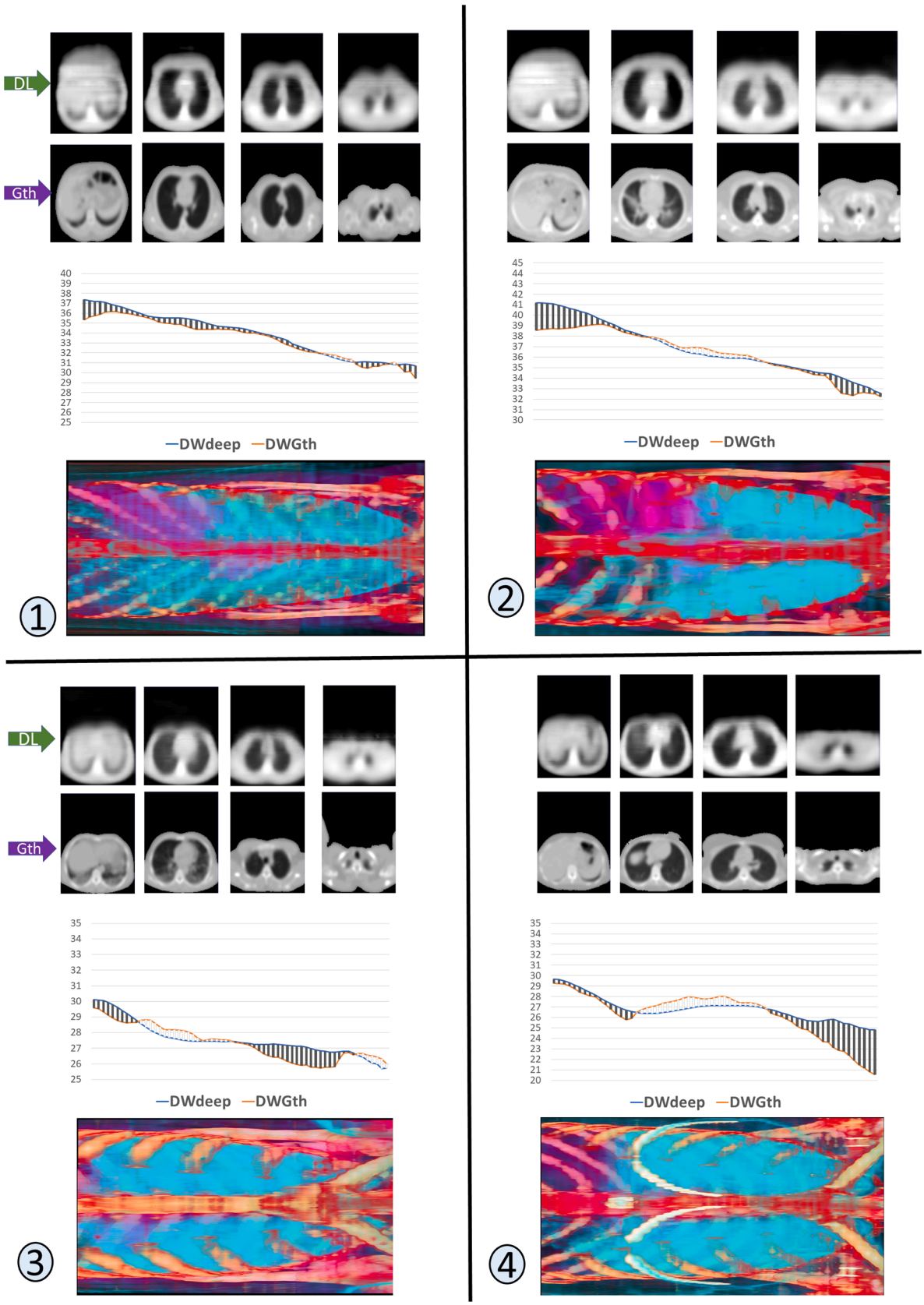

Fig. 2. Four examples of DL performance. For each case, the upper row is the DL output, the second row is the ground truth image. In the bottom, the perpendicular black lines show the slicewise difference between DW calculated by deep learning (orange line) and ground truth (blue line). The last row shows the 3D colored visualization of images where the blue volume depicts the lung. Case #1: male patient with BMI > 30. Case #2: female patient with BMI > 30. Case #3: male patient with BMI < 30. Case #4: female patient with BMI < 30.

Table 2
Results of DL measurements of two additional external test groups. ABS: Absolute. E: Error. S: Slicewise strategy. T: Total strategy.

	138 cases							648 cases						
Value	**Area-E-S(%)**	**HU_AE (HU)**	**DICE-S**	**DW-E-S(%)**	**DW-E-T(%)**	**DW-ABS-E-T(%)**	**DW-E-T (mm)**	**Area-E-S(%)**	**HU_AE (HU)**	**DICE-S**	**DW-E-S(%)**	**DW-E-T(%)**	**DW-ABS-E-T(%)**	**DW-E-T (mm)**
Average	5.2	55.1	0.936	11.3	3.7	4.7	10.9	4	51.5	0.948	9.6	2.9	3.7	8.6
min	0.7	0.3	0.783	2	−6.2	0	−17.5	0.6	0.4	0.783	1.1	−9.2	0	−35.4
per 5	1.3	4.6	0.887	4	−3.7	0.5	−11	1.3	4.8	0.916	3.5	−3.1	0.3	−9.4
per 10	2	8.6	0.899	5.1	−1.7	0.7	−5.2	1.6	9.8	0.926	4.3	−1.8	0.6	−5.4
per 25	2.7	30.0	0.930	6.8	0.7	1.8	1.8	2.4	23.3	0.937	5.9	0.4	1.5	1
per 50	4.1	56.3	0.940	9.4	3.9	4.1	11.8	3.5	47.2	0.950	8.5	2.8	3.2	8.4
per 75	6.4	79.3	0.958	13.8	6.3	6.3	19.4	5	73.6	0.961	12	5.3	5.4	16.4
per 90	9.2	96.2	0.966	20.4	9.6	9.6	26.9	6.7	100.1	0.969	16.8	7.7	7.8	23.1
per 95	13.1	111.4	0.968	23.8	11	11	31.5	8.4	112.4	0.973	19.5	9	9.1	27.7
max	24.2	150.8	0.976	36.2	16.6	16.6	45.5	24.2	197.8	0.984	36.2	16.6	16.6	45.5
stdev	3.6	34.3	0.030	6.3	4.4	3.4	12.7	2.5	35.0	0.020	5.2	3.7	2.8	11.2
Q1-Q3	3.6	49.2	0.028	7	5.6	4.5	17.5	2.7	50.4	0.023	6.1	4.9	3.8	15.4

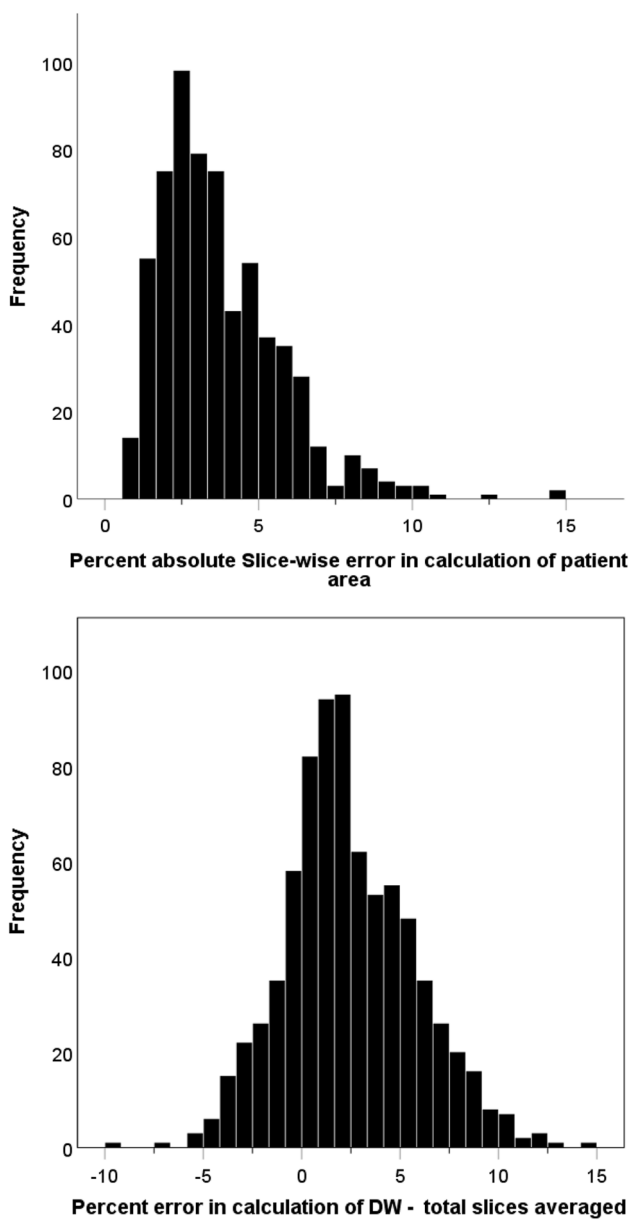

Fig. 3. Histogram of the distribution of the percentage error in the area measurement from the deep predicted images in slice-wise approach (upper figure), and DW calculation from deep predicted images (lower figure).

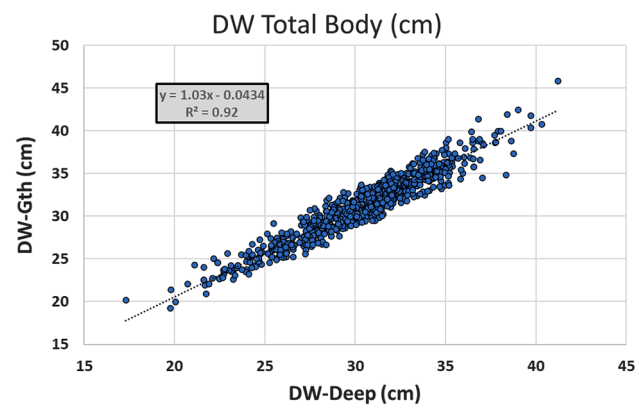

Fig. 4. Correlation between the total DW calculated using the proposed DL approach and ground truth images.

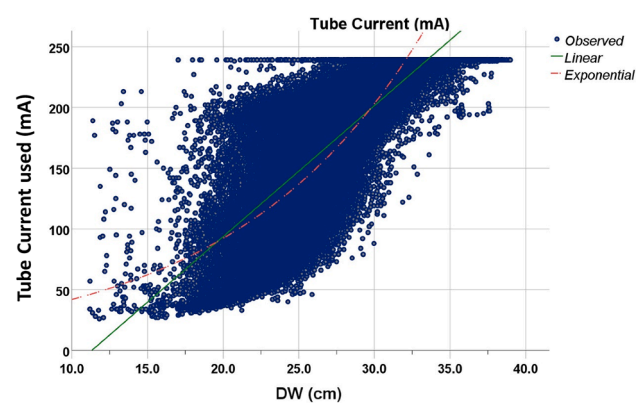

Fig. 5. Trend of tube current adjustment with respect to DW in all cases scanned with 110 kVp. Each point is related to a single slice. The fitted linear (solid-green) and exponential (dashed-red) curves are also shown.

a solution to calculate DW unaffected by the truncation problem. Repeating the reconstruction with a larger field of view is not usually possible as the raw data are not available. Three main barriers in the automated DW calculation from the localizer images are calibration of the pixel intensities, magnification, and mis-centering issues, which lead to inaccurate and unreproducible measurements. In this study, we trained a network to reconstruct the axial images by considering the pixel values in the localizer to overcome the time-consuming and prone to error calibration procedure. Moreover, this approach generates valuable information regarding the shape and size of the patient prior to

the axial scan. The performance of the body contour segmentation approach (Dice coefficient = 0.95) was comparable to previous studies reported by Juszczyk et al. [31] and Anam et al. [32], achieving a Dice coefficient of 0.98 to 0.99, respectively. It is worth emphasizing that they used 3D axial images, while our model relied on a single slice AP localizer as the input image. Furthermore, we demonstrated the robustness of our method with respect to table height and magnification variations on 138 unseen external validation datasets. Nine cases in the test dataset were scanned twice at two different table heights. These patients were included in the two groups of patients with fixed and varied table heights. The table height for these patients in the test dataset varied from 103 to 179 mm. Considering the quantitative metrics, no dramatic changes were observed for the patients scanned twice at different table heights. The errors between the two scans with different table heights were within the range of errors (standard deviation) across the patients scanned at a fixed table height. The average change in these nine cases were 1.65 %, 0.01 %, 2.36 %, 4.40 %, and 1.49 % in terms of Area-E-S (%), DICE-S, DW-E-S (%), DW-E-T (mm), DW-E-T (%), respectively, which is comparable to the average changes across subjects scanned at a fixed table height of 160 mm. It should be noted that the positioning, scan range, and other parameters were different between the two scans. Hence, the variation in model performance is not solely related to table height. The similar results obtained from the same patient scanned twice at different table heights demonstrate the generalizability and robustness of the model to changes in table height.

In addition, the prediction of patient size-related information from the localizer images, commonly acquired in extended axial FOVs compared to the axial CT images, is helpful for the selection of the best fit computational phantom either in full Monte Carlo simulations [33] or other pre-tabulated CT dose calculation software, such as ImPactCT or NCICT [34,35] dose engines. The DW or patient's effective diameter is required to calculate the SSDE as a more personalized metric rather than the CTDIvol. Our proposed model can be useful in the calculation of SSDE, especially when the DW calculated from 3D axial images is not reliable, e.g. in the case of truncated CT reconstructions or raw data not available.

One of the most critical applications of the extracted metrics from the scout scans before the spiral CT acquisition in 64 slices in the CC direction is optimizing the acquisition protocol to reduce radiation exposure according to body shape, size, and attenuation properties. The only parameter considered by automatic TCM or kVp selection software on current commercial CT scanners is attenuation-related information from a single projection [36]. We trained a model to provide the attenuation information from a single projection angle. The required time for preprocessing, inference, and post-processing (measurement of the metrics) for a new case is in the order of a few seconds, making the technique applicable in the clinical routine. We also calculated slice-wise errors (comparing the outcomes slice-by-slice to the GT) to investigate the possibility of object-specific acquisition parameters optimization. The calculated shape and attenuation parametrics of body contour and DW can be helpful in calibrating both angular and Z-axis tube current modulation according to the specific body of the patient.

As shown in Fig. 5, the adaptation of tube current to DW is not well established in the clinical setting [37]. The scanner chooses the desired tube current based on the localizer image variation in the Z direction and mainly based on the calibration data between the localizer pixel value and the roughly estimated attenuation characteristics of the patient's body with no knowledge about the shape. This procedure could be affected by different issues such as patient mis-centering or acquisition parameters [37]. A number of studies attempted to locate the patient automatically by means of external cameras to overcome the mis-centering problem. Although these devices are capable of pinpointing the patient size and body contour with clothes, they do not provide any information about body composition. Moreover, they are prone to significant errors when patients are covered with blankets or bed sheets. Nevertheless, these devices usually provide better performance compared to technologists [38–41]. Employing the proposed deep learning-based solution with automatic patient positioning systems would be optimal for DW determination before the spiral scan. This fact proves the need for methods, such as the one proposed in this study in a clinical setting. The maximum allowed tube current according to the protocol selected by the technologist (250 mA) limited the performance of the TCM system (Fig. 5). Even for very large and highly attenuating patient body parts, the maximum tube current was 250 mA. AP localizer is more popular or frequently used than the lateral localizer in clinical practice owing to the better visualization to localize organs and delimitate the scan range. It has been shown that the localizer image is prone to less error due to mis-centering and can help the TCM to select more appropriate tube currents [39]. In this regard, even by considering the additional lateral localizer radiation exposure, the total radiation from the CT scan can be reduced [42]. Employing two AP and lateral scout views would lead to less changes in the CTDI due to varying magnification. Li et al. [43] scanned patients and a CTDI cylindrical phantom on a GE light speed scanner and changed the table height. They reported 12–49 % change in the CTDI by changing the table height. Euler et al. [44] scanned a pediatric CIRS phantom at different table heights by acquiring two AP and lateral localizers. They reported 34 % change in organ doses and 26 % change in tube current when moving the table in the vertical direction. Kaasalainen et al. [45]demonstrated that much less change in CTDIvol would be observed when using a lateral localizer (29 %) compared to AP localizer (91 %). The lateral scout view exhibited superior robustness to changes in table height and/or magnification. Despite the superiority of lateral to AP scout view, variation in tube current of up to 30 % was observed. In this regard, the proposed method exhibited a mean error of 4.7 % (0 to 16.6 %) in DW measurement, demonstrating its robustness against changes in table height.

In terms of accuracy, despite the slightly smoothed appearance of the estimated images (Fig. 2), our results are comparable or superior to recently published studies with an average HU_AE of 52 HUs. Anam et al. reported 5.4 ± 4.2 % and 2.3 ± 3.2 % errors in calculating T_W in an anthropomorphic phantom study and 30 clinical cases, respectively [10]. Our results showed similar R^2 achieved by the proposed metric compared to Burton et al.[24], wherein they used both AP and lateral images simultaneously. We only used a single AP localizer commonly acquired in clinical protocols. Moreover, better than Mihalidis et al. [13] proposed technique, they calculated DW from the 16 axial chest CT images with a less computational burden to achieve an accuracy of 13 % compared to the AAPM 220 guidelines. In two consecutive studies, Zhang et al. [21,22] achieved an accuracy of ± 2.5 % in terms of DW for patients with 25 to 30 cm DW through calibrating localizer pixel intensities for multiple scanner vendors. Our results showed a correlation between the error and patient size, where larger patients have more considerable errors than smaller patients. To compare our results with Zhang et al., we selected 292 patients with sizes smaller than 30 cm, the DW error and absolute DW error were 1.7 ± 3.4 % and 2.9 ± 2.4 %, respectively. In comparison, our method estimated the body contour size and DW from a single measurement. We included a large number of clinical studies in contrast to previous studies where phantom measurements were extended on a selected and limited number of patients.

We excluded 8 cases from our dataset identified as outliers, representing 1.3 % of the test dataset. Rather unusual body habitus of patients can be seen in Supplementary Fig. 1. The skinny border of the anterior chest wall led to successful body contouring from the predicted image. The automatic body contour segmentation on the original axial images produced acceptable results. From a total of 3243 cases, only one case was edited after visual inspection.

This work bears some limitations that should be acknowledged. First, only chest CT images were investigated. Second, we provided a model for a single vendor. Yet, we believe the model can be easily transferred and implemented on other scanners provided sufficient training data are available. Inter-scanner variability of the localizer pixel values limits the

application of this model. The localizer pixel value is related to the total attenuation across the patient body and the table along the path of the X-ray source to the detector. The localizer images are processed to enhance/optimize the quality/contrast of visualization. In this light, the localizer pixel values are not quantitative and standardized, since they are not used for diagnostic purposes. To create a quantitative CT localizer, similar to Hounsfield unit standard values in spiral 3D images, time-consuming phantom calibrations are required, which is dependent on the phantom shape and size. Since the geometry and pixel intensities of the localizer are vendor-specific, it is not reasonable to test the current model on other scanners. An experimental study involving scanning an anthropomorphic phantom at variable table heights to compare the DL-based calculated DW with the ground truth may be helpful to demonstrate the robustness of the model against changes in table height. Unfortunately, this was not possible in the present study. Moreover, as reported by Perisinakis et al. [46], the radiographer might select spiral scan ranges beyond the craniocaudal region which is included in the scout scan. This acquisition is not recommended since there is no information about the size/attenuation characteristics of the patient's body to guide the TCM system in selecting the tube current. Our proposed model is not capable of predicting patient's shape or DW in this case.

5. Conclusion

We developed a DL model to predict axial images from a single 2D AP localizer image. Our DL-based proposed method is able to simultaneously estimate the shape, size, and attenuation parameters with acceptable slice-wise accuracy, robust to patient mis-centering and truncation, and applicable to extended axial field-of-view scans. This information could be used to measure the radiation dose in terms of SSDE, phantom selection for Monte Carlo-based calculations or a pre-tabulated software, and more importantly, for protocol optimization in chest CT imaging.

Declaration of Competing Interest

The authors declare that they have no known competing financial interests or personal relationships that could have appeared to influence the work reported in this paper.

Acknowledgments

This work was supported by the Euratom research and training programme 2019-2020 Sinfonia project under grant agreement No 945196.

Appendix A. Supplementary data

Supplementary data to this article can be found online at https://doi.org/10.1016/j.ejrad.2022.110602.

References

[1] H. Alkadhi, A. Euler, The future of Computed Tomography: Personalized, functional, and precise, Invest. Radiol. 55 (9) (2020) 545–555.
[2] Y. Inoue, K. Nagahara, Y. Tanaka, H. Miyatake, H. Hata, T. Hara, Methods of CT dose estimation in whole-body 18F-FDG PET/CT, J. Nucl. Med. 56 (5) (2015) 695–700.
[3] H. Abdollahi, I. Shiri, Y. Salimi, M. Sarebani, R. Mehdinia, M.R. Deevband, S. R. Mahdavi, A. Sohrabi, A. Bitarafan-Rajabi, Radiation dose in cardiac SPECT/CT: An estimation of SSDE and effective dose, Eur. J. Radiol. 85 (12) (2016) 2257–2261.
[4] Y. Salimi, M. Deevband, P. Ghafarian, M. Ay, Uncertainties in effective dose estimation for CT transmission scan in total body PET-CT imaging with Auto mA3D tube current modulation, Int. J. Radiat. Res. 16 (4) (2018) 465–472.
[5] I. Shiri, A. Akhavanallaf, A. Sanaat, Y. Salimi, D. Askari, Z. Mansouri, S. P. Shayesteh, M. Hasanian, K. Rezaei-Kalantari, A. Salahshour, S. Sandoughdaran, H. Abdollahi, H. Arabi, H. Zaidi, Ultra-low-dose chest CT imaging of COVID-19 patients using a deep residual neural network, Eur. Radiol. 31 (3) (2021) 1420–1431.
[6] C.H. McCollough, S. Leng, L. Yu, D.D. Cody, J.M. Boone, M.F. McNitt-Gray, CT dose index and patient dose: they are not the same thing, Radiology 259 (2) (2011) 311–316.
[7] AAPM, Use of Water Equivalent Diameter for Calculating Patient Size and Size-Specific Dose Estimates (SSDE) in CT, AAPM, 2014.
[8] ICRP, ICRP Publication 135: Diagnostic Reference Levels in Medical Imaging., Ann ICRP 46(1) (2017) 1-144.
[9] J. Xu, X. Wang, H. Xiao, J. Xu, Size-specific dose estimates based on water-equivalent diameter and effective diameter in Computed Tomography coronary angiography, Med. Sci. Monitor : Int. Med. J. Experim. Clin. Res. 25 (2019) 9299–9305.
[10] C. Anam, F. Haryanto, R. Widita, I. Arif, G. Dougherty, The size-specific fose estimate (SSDE) for truncated computed tomography images, Radiat. Prot. Dosim. 175 (3) (2017) 313–320.
[11] C. Anam, F.R. Mahdani, W.K. Dewi, H. Sutanto, P. Triadyaksa, F. Haryanto, G. Dougherty, An improved method for automated calculation of the water-equivalent diameter for estimating size-specific dose in CT, J. Appl. Clin. Med. Phys. 22 (9) (2021) 313–323.
[12] A. Daudelin, D. Medich, S.Y. Andrabi, C. Martel, Comparison of methods to estimate water-equivalent diameter for calculation of patient dose, J. Appl. Clin. Med. Phys. 19 (5) (2018) 718–723.
[13] D. Mihailidis, V. Tsapaki, P. Tomara, A simple manual method to estimate water-equivalent diameter for calculating size-specific dose estimate in chest computed tomography, Br. J. Radiol. 94 (1117) (2021) 20200473.
[14] P. Nowik, G. Poludniowski, A. Svensson, R. Bujila, F. Morsbach, T.B. Brismar, The synthetic localizer radiograph - A new CT scan planning method, Phys. Med. 61 (2019) 58–63.
[15] C.P. Favazza, L. Yu, S. Leng, J.M. Kofler, C.H. McCollough, Automatic exposure control systems designed to maintain constant image noise: effects on computed tomography dose and noise relative to clinically accepted technique charts, J. Comput. Assist. Tomogr. 39 (3) (2015) 437–442.
[16] M. Fukunaga, K. Matsubara, S. Ichikawa, H. Mitsui, H. Yamamoto, T. Miyati, CT dose management of adult patients with unknown body weight using an effective diameter, Eur. J. Radiol. 135 (2021), 109483.
[17] S. Cournane, E. Brunell, M. Rowan, Establishing how patient size and degree of miscentring affect CTDI(vol), using patient data from a dose tracking system, Br. J. Radiol. 92 (1099) (2019) 20180992.
[18] S. Ichikawa, M. Hamada, H. Sugimori, A deep-learning method using computed tomography scout images for estimating patient body weight, Sci. Rep. 11 (1) (2021) 15627.
[19] K. Kuriyama, K. Matsubara, S. Hisahara, Y. Nagata, R. Nosaka, R. Goto, N. Yanano, K. Shimizu, T. Shoji, Effect of table height displacement and patient center deviation on size-specific dose estimates calculated from computed tomography localizer radiographs, Phys. Eng. Sci. Med. 43 (2) (2020) 665–672.
[20] M. Terashima, K. Mizonobe, H. Date, Determination of appropriate conversion factors for calculating size-specific dose estimates based on X-ray CT scout images after miscentering correction, Radiol. Phys. Technol. 12 (3) (2019) 283–289.
[21] D. Zhang, G. Mihai, L.G. Barbaras, O.R. Brook, M.R. Palmer, A new method for CT dose estimation by determining patient water equivalent diameter from localizer radiographs: Geometric transformation and calibration methods using readily available phantoms, Med. Phys. 45 (7) (2018) 3371–3378.
[22] D. Zhang, X. Liu, X. Duan, A.A. Bankier, J. Rong, M.R. Palmer, Estimating patient water equivalent diameter from CT localizer images – A longitudinal and multi-institutional study of the stability of calibration parameters, Med. Phys. 47 (5) (2020) 2139–2149.
[23] C. Anam, T. Fujibuchi, T. Toyoda, N. Sato, F. Haryanto, R. Widita, I. Arif, G. Dougherty, A simple method for calibrating pixel values of the CT localizer radiograph for calculating water-equivalent diameter and size-specific dose estimate, Radiat. Prot. Dosim. 179 (2) (2018) 158–168.
[24] C.S. Burton, Method of determining geometric patient size surrogates using localizer images in CT, J. Appl. Clin. Med. Phys. 21 (3) (2020) 178–183.
[25] H. Arabi, A. AkhavanAllaf, A. Sanaat, I. Shiri, H. Zaidi, The promise of artificial intelligence and deep learning in PET and SPECT imaging, Physica Med. 83 (2021) 122–137.
[26] S.A. Harmon, T.H. Sanford, S. Xu, E.B. Turkbey, H. Roth, Z. Xu, D. Yang, A. Myronenko, V. Anderson, A. Amalou, M. Blain, M. Kassin, D. Long, N. Varble, S. M. Walker, U. Bagci, A.M. Ierardi, E. Stellato, G.G. Plensich, G. Franceschelli, C. Girlando, G. Irmici, D. Labella, D. Hammoud, A. Malayeri, E. Jones, R. M. Summers, P.L. Choyke, D. Xu, M. Flores, K. Tamura, H. Obinata, H. Mori, F. Patella, M. Cariati, G. Carrafiello, P. An, B.J. Wood, B. Turkbey, Artificial intelligence for the detection of COVID-19 pneumonia on chest CT using multinational datasets, Nat. Commun. 11 (1) (2020) 4080.
[27] O. Schoppe, C. Pan, J. Coronel, H. Mai, Z. Rong, M.I. Todorov, A. Muskes, F. Navarro, H. Li, A. Erturk, B.H. Menze, Deep learning-enabled multi-organ segmentation in whole-body mouse scans, Nat. Commun. 11 (1) (2020) 5626.
[28] I. Shiri, H. Arabi, Y. Salimi, A.H. Sanaat, A. Akhavanalaf, G. Hajianfar, D. Askari, S. Moradi, Z. Mansouri, M. Pakbin, S. Sandoughdaran, H. Abdollahi, A.R. Radmard, K. Rezaei-Kalantari, M.G. Oghli, H. Zaidi, COLI-NET: Fully Automated COVID-19 Lung and Infection Pneumonia Lesion Detection and Segmentation from Chest CT Images, medRxiv (2021) 2021.04.08.21255163.
[29] I. Shiri, Y. Salimi, A. Saberi, M. Pakbin, G. Hajianfar, A.H. Avval, A. Sanaat, A. Akhavanallaf, S. Mostafaei, Z. Mansouri, D. Askari, M. Ghasemian, E. Sharifipour, S. Sandoughdaran, A. Sohrabi, E. Sadati, S. Livani, P. Iranpour, S. Kolahi, B. Khosravi, M. Khateri, S. Bijari, M.R. Atashzar, S.P. Shayesteh, M.R. Babaei, E.

Jenabi, M. Hasanian, A. Shahhamzeh, S.Y.F. Gholami, A. Mozafari, H. Shirzad-Aski, F. Movaseghi, R. Bozorgmehr, N. Goharpey, H. Abdollahi, P. Geramifar, A.R. Radmard, H. Arabi, K. Rezaei-Kalantari, M. Oveisi, A. Rahmim, H. Zaidi, Diagnosis of COVID-19 Using CT image Radiomics Features: A Comprehensive Machine Learning Study Involving 26,307 Patients, medRxiv (2021) 2021.12.07.21267367.

[30] I. Shiri, Y. Salimi, M. Pakbin, G. Hajianfar, A.H. Avval, A. Sanaat, S. Mostafaei, A. Akhavanallaf, A. Saberi, Z. Mansouri, D. Askari, M. Ghasemian, E. Sharifipour, S. Sandoughdaran, A. Sohrabi, E. Sadati, S. Livani, P. Iranpour, S. Kolahi, M. Khateri, S. Bijari, M.R. Atashzar, S.P. Shayesteh, B. Khosravi, M.R. Babaei, E. Jenabi, M. Hasanian, A. Shahhamzeh, S.Y.F. Gholami, A. Mozafari, A. Teimouri, F. Movaseghi, A. Ahmari, N. Goharpey, R. Bozorgmehr, H. Shirzad-Aski, R. Mortazavi, J. Karimi, N. Mortazavi, S. Besharat, M. Afsharpad, H. Abdollahi, P. Geramifar, A.R. Radmard, H. Arabi, K. Rezaei-Kalantari, M. Oveisi, A. Rahmim, H. Zaidi, COVID-19 Prognostic Modeling Using CT Radiomic Features and Machine Learning Algorithms: Analysis of a Multi-Institutional Dataset of 14,339 Patients, medRxiv (2021) 2021.12.07.21267364.

[31] J. Juszczyk, P. Badura, J. Czajkowska, A. Wijata, J. Andrzejewski, P. Bozek, M. Smolinski, M. Biesok, A. Sage, M. Rudzki, W. Wieclawek, Automated size-specific dose estimates using deep learning image processing, Med. Image Anal. 68 (2021), 101898.

[32] C. Anam, F. Haryanto, R. Widita, I. Arif, G. Dougherty, Automated calculation of water-equivalent diameter (DW) based on AAPM Task Group 220, J. Appl. Clin. Med. Phys. 17 (4) (2016) 320–333.

[33] A. Akhavanallaf, T. Xie, H. Zaidi, Assessment of uncertainties associated with Monte Carlo-based personalized dosimetry in clinical CT examinations, Phys. Med. Biol. 65 (4) (2020), 045008.

[34] C. Lee, K.P. Kim, W.E. Bolch, B.E. Moroz, L. Folio, NCICT: a computational solution to estimate organ doses for pediatric and adult patients undergoing CT scans, J. Radiol. Prot. 35 (4) (2015) 891–909.

[35] B. Newman, A. Ganguly, J.E. Kim, T. Robinson, Comparison of different methods of calculating CT radiation effective dose in children, AJR Am. J. Roentgenol. 199 (2) (2012) W232–W239.

[36] M.K. Kalra, M.M. Maher, T.L. Toth, B. Schmidt, B.L. Westerman, H.T. Morgan, S. Saini, Techniques and applications of automatic tube current modulation for CT, Radiology 233 (3) (2004) 649–657.

[37] D. Merzan, P. Nowik, G. Poludniowski, R. Bujila, Evaluating the impact of scan settings on automatic tube current modulation in CT using a novel phantom, Br. J. Radiol. 90 (1069) (2017) 20160308.

[38] R. Booij, M. van Straten, A. Wimmer, R.P.J. Budde, Automated patient positioning in CT using a 3D camera for body contour detection: accuracy in pediatric patients, Eur. Radiol. 31 (1) (2021) 131–138.

[39] B. Dane, T. O'Donnell, S. Liu, E. Vega, S. Mohammed, V. Singh, A. Kapoor, A. Megibow, Radiation dose reduction, improved isocenter accuracy and CT scan time savings with automatic patient positioning by a 3D camera, Eur. J. Radiol. 136 (2021), 109537.

[40] N. Saltybaeva, B. Schmidt, A. Wimmer, T. Flohr, H. Alkadhi, Precise and Automatic Patient Positioning in Computed Tomography: Avatar Modeling of the Patient Surface Using a 3-Dimensional Camera, Invest. Radiol. 53 (11) (2018) 641–646.

[41] J. Greffier, J. Frandon, H. De Forges, A. Hamard, A. Belaouni, J.B. Wahl, D. Dabli, J.P. Beregi, Impact of additional mattresses in emergency CT on the automated patient centering proposed by a 3D camera: a phantom study, Sci. Rep. 11 (1) (2021).

[42] Y. Salimi, I. Shiri, A. Akhavanallaf, Z. Mansouri, A. Saberi Manesh, A. Sanaat, M. Pakbin, D. Askari, S. Sandoughdaran, E. Sharifipour, H. Arabi, H. Zaidi, Deep learning-based fully automated Z-axis coverage range definition from scout scans to eliminate overscanning in chest CT imaging, Insights Imaging 12 (1) (2021) 162.

[43] J. Li, U.K. Udayasankar, T.L. Toth, J. Seamans, W.C. Small, M.K. Kalra, Automatic patient centering for MDCT: effect on radiation dose, AJR Am. J. Roentgenol. 188 (2) (2007) 547–552.

[44] A. Euler, N. Saltybaeva, H. Alkadhi, How patient off-centering impacts organ dose and image noise in pediatric head and thoracoabdominal CT, Eur. Radiol. 29 (12) (2019) 6790–6793.

[45] T. Kaasalainen, T. Makela, M. Kortesniemi, The effect of vertical centering and scout direction on automatic tube voltage selection in chest CT: a preliminary phantom study on two different CT equipments, Eur J Radiol Open 6 (2019) 24–32.

[46] K. Perisinakis, N. Ntoufas, M. Velivassaki, A. Tzedakis, M. Myronakis, A. Hatzidakis, J. Damilakis, Effect of scan projection radiography coverage on tube current modulation in pediatric and adult chest CT, Zeitschrift für Medizinische Physik 30 (4) (2020) 259–270.